Available online at www.sciencedirect.com

SciVerse ScienceDirect

Ceramics International 38 (2012) 1843–1849

CERAMICS INTERNATIONAL

www.elsevier.com/locate/ceramint

Rheological properties of aqueous alumina–alumina-doped Y-PSZ suspensions

Heidy L. Calambás Pulgarin, Liliana B. Garrido, María P. Albano *

Centro de Tecnología de Recursos Minerales y Cerámica (CETMIC), C.C. 49 (B1897ZCA) M. B. Gonnet, Provincia de Buenos Aires, Argentina

Received 23 June 2011; received in revised form 29 September 2011; accepted 3 October 2011
Available online 8 October 2011

Abstract

The effect of the substitution of alumina (Al_2O_3) by 0.3 wt% Al_2O_3-doped 3 mol% yttria-partially stabilized zirconia (Y-PSZ) on the rheological properties of concentrated aqueous slips was studied. Al_2O_3–Al_2O_3-doped Y-PSZ aqueous suspensions with different Al_2O_3-doped Y-PSZ contents: 0, 22 and 50 vol% were prepared using ammonium polyacrylate (NH_4PA) as dispersant. The particle size distributions of Al_2O_3 and Al_2O_3-doped Y-PSZ powders were similar; however, the particle shape and the surface coating of alumina conferred a markedly higher specific surface area to the Al_2O_3-doped Y-PSZ powder. The substitution of Al_2O_3 by Al_2O_3-doped Y-PSZ in the mixtures decreased the negative surface charge of the powders at pH 9, thereby increasing the amount of NH_4PA adsorbed and consequently the electrosteric repulsion between particles. However, the viscosity and yield stress values increased with increasing Al_2O_3-doped Y-PSZ content for all the solid loading studied. This could be explained by a larger interaction size of the Al_2O_3-doped Y-PSZ particles which resulted in a higher effective volume solid fraction and a lower amount of free-liquid available for flow.

Keywords: Al_2O_3–Al_2O_3-doped Y-PSZ suspensions; Dispersion; Rheological properties

1. Introduction

Recently, zirconia-toughened-alumina ceramics have received considerable attention due to their attractive properties, including high-temperature mechanical strength, good thermal shock resistance, wear and oxidation resistance, low thermal conductivity, and the close match between their thermal expansion coefficients and those of metals [1,2]. These properties make zirconia–alumina ceramics suitable for a variety of high demanding applications including dental screws, cutting blades, electrosurgical insulators, valve seals, body armor, pump components, oxygen sensors, dies, and prosthesis components such as hip joints [3,4]. The zirconia grains embedded in an alumina matrix enhance the flexural strength, fracture toughness, and fatigue resistance [5]. The toughening mechanisms identified in zirconia-reinforced alumina ceramics is attributed to the stress induced phase transformation of metastable tetragonal grains towards the monoclinic symmetry ahead of a propagating crack, leading to an increase in the work of fracture [5]. This phenomenon of transformation toughening relies on the volume expansion, 3–5%, and shear strain ≈7% develops when tetragonal zirconia transforms to the monoclinic form [6]. Besides, microcracks extending in the stress field of a propagating crack can absorb the fracture energy, increasing the material toughness by the microcrack toughening mechanism [2]. However, studies on the application of these materials in humid environment at low temperature have shown that the tetragonal → monoclinic transformation can also be induced at the surface of ZrO_2 grains, leading to the so-called hydrothermal transformation [3] which produces a slow degradation of the composite mechanical properties. In order to reduce the ZrO_2 susceptibility to the hydrothermal instability, 3 mol% yttria-partially stabilized zirconia powder doped with 0.3 wt% Al_2O_3 was used.

Colloidal shaping methods enable to achieve high microstructural homogeneity in green and sintered parts, and offer near-net-shaping capabilities that reduce the postsintering machining operations and the production costs [2]. The first step in the colloidal process, is the preparation of stable concentrated aqueous suspensions of the ceramic powders.

* Corresponding author. Tel.: +54 0221 484 0247; fax: +54 0221 471 0075.
E-mail address: palbano@cetmic.unlp.edu.ar (M.P. Albano).

0272-8842/$36.00
doi:10.1016/j.ceramint.2011.10.009

At high solids loading, relatively low slip viscosity can only be achieved in the presence of an optimum dispersion state of particles. Anionic polyelectrolytes such as NH_4PA are commonly used as dispersant of ceramic powders in aqueous media [7]. The polyelectrolyte adsorbs at the solid–liquid interface and infers repulsive forces between the particles which keeps them well dispersed; the repulsive interactions are caused by electrostatic and steric effects [8]. The dispersion properties of aqueous Al_2O_3–0.3 wt% Al_2O_3-doped Y-PSZ suspensions with NH_4PA have not been reported in the literature. Therefore, the influence of 0.3 wt% Al_2O_3-doped Y-PSZ concentration on the rheological properties of aqueous Al_2O_3–0.3 wt% Al_2O_3-doped Y-PSZ suspensions and the particle packing ability during sedimentation were studied.

2. Experimental procedure

2.1. Materials

Alumina (A16 SG, Alcoa Chemicals, USA) and 3 mol% yttria-partially stabilized zirconia with 0.3 wt% Al_2O_3 (Saint-Gobain ZirPro, Chine) powders were used in this study. Al_2O_3–Al_2O_3-doped Y-PSZ mixtures with two compositions were prepared: Al_2O_3 (78 vol%)–Al_2O_3-doped Y-PSZ (22 vol%) and Al_2O_3 (50 vol%)–Al_2O_3-doped Y-PSZ (50 vol%). A commercial ammonium polyacrylate solution (Duramax D 3500, Rohm & Haas, Philadelphia, PA) was used as deflocculant.

2.2. Powder characterization

The specific surface area (S_g) and the particle size distribution of the powders were measured using a Micromeritics Accusorb and a Sedigraph (Micromeritics), respectively. The morphological features of the powders were examined by scanning electron microscopy (SEM) (JEOL, JSM-6360). To determinate the isoelectric point (IEP) of the powders, zeta potential measurements were carried out with an instrument Zetasizer nano ZS (Malvern Instruments, UK). Zeta potential against pH curves were determined for 0.05 vol% slips of different powders: Al_2O_3, Al_2O_3-doped Y-PSZ, Al_2O_3 (78 vol%)–Al_2O_3-doped Y-PSZ (22 vol%) and Al_2O_3 (50 vol%)–Al_2O_3-doped Y-PSZ (50 vol%) in the pH range 3–10. The pH adjustment was achieved with HCl or KOH solutions. The dispersion of Al_2O_3 and Al_2O_3-doped Y-PSZ powders at different pH values was studied by measuring the mean particle diameter of 2 vol% suspensions as a function of pH.

2.3. Slip preparation

35 vol% aqueous Al_2O_3, Al_2O_3 (78 vol%)–Al_2O_3-doped Y-PSZ (22 vol%) and Al_2O_3 (50 vol%)–Al_2O_3-doped Y-PSZ (50 vol%) slips with various amounts of deflocculant were prepared by suspending particles in deionized water via 40 min of ultrasound; the pH was manually adjusted to be maintained at 9 with ammonia (25%). In addition, slips with the optimum NH_4PA concentration and different solid contents were prepared at pH 9 to study the influence of the solid loading on the rheological properties.

2.4. NH_4PA adsorption and zeta potential measurements

In order to determine the amount of NH_4PA adsorbed, different 35 vol% slips with the optimum NH_4PA concentration were centrifuged for 30 min at 2500 rpm and washed twice with distilled water. Then, the solid was dried at 100 °C and analyzed by thermal gravimetric analysis (TGA) (Model STA 409, Netzsch, Inc., Germany) at a heating rate of 10 °C/min in air. The TGA data showed a water weight loss at temperatures near 100 °C and a weight loss due to the NH_4PA decomposition in a temperature range from 300 °C to 600 °C. This weight loss was used to determine the amount of NH_4PA adsorbed on each sample. Although the adsorption data obtained with this technique were semiquantitative, they provided a relative measure of the amount of NH_4PA adsorbed on the samples.

Zeta potential versus pH curves were determined for 0.05 vol% slips of different powders: Al_2O_3, Al_2O_3 (78 vol%)–Al_2O_3-doped Y-PSZ (22 vol%) and Al_2O_3 (50 vol%)–Al_2O_3-doped Y-PSZ (50 vol%) with the optimum amount of NH_4PA in the pH range 3–10.

2.5. Slip characterization

Steady state flow curves of Al_2O_3, Al_2O_3 (78 vol%)–Al_2O_3-doped Y-PSZ (22 vol%) and Al_2O_3 (50 vol%)–Al_2O_3-doped Y-PSZ (50 vol%) slips were performed by measuring the steady shear stress value as a function of shear rate in the range of 0.5–542 s^{-1}using a concentric cylinder viscometer (Haake VT550, Germany) at 25 °C. A coaxial cylinder system with two gaps (sensor system NV Haake) was used. As soon as stationary conditions were reached at each shear rate, the shear rate increased in steps up to the maximum value and then decreased. The majority of the curves did not show hysteresis area.

The slips were allowed to settle under gravity, the volume fraction of sediment was measured after 40 days; this value was used to calculate the maximum packing fraction.

3. Results and discussion

3.1. Powder characterization

The specific surface area of Al_2O_3 and 0.3 wt% Al_2O_3-doped Y-PSZ powders was 8.74 and 12.25 m^2/g, respectively. The particle size distribution curves of Al_2O_3 and Al_2O_3-doped Y-PSZ powders were similar (Fig. 1). Alumina showed an unimodal distribution with particle diameters >0.1 and <0.75 μm, the more frequent particle diameters were in the range 0.15–0.3 μm. A slightly narrow particle size distribution was found for Al_2O_3-doped Y-PSZ; thus a greater volume of finer particles (diameters between 0.10 and 0.20 μm) and a lesser volume of particles with diameters in the range 0.20–0.55 μm were observed, the more frequent particle diameter was 0.15 μm.

Fig. 2a and b shows SEM micrographs of Al_2O_3 and Al_2O_3-doped Y-PSZ powders, respectively. The shape of Al_2O_3-doped

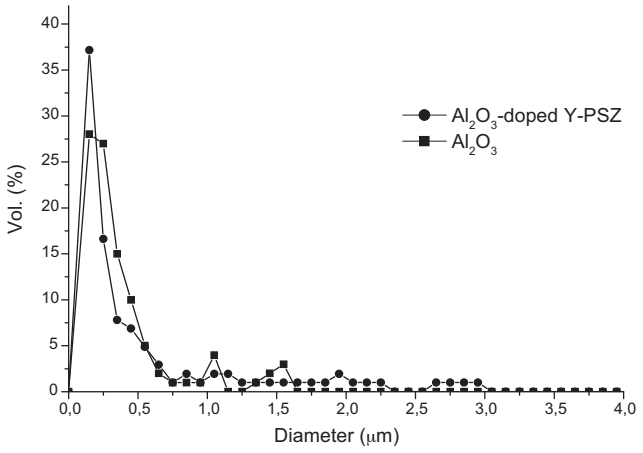

Fig. 1. Particle size distribution curves of different powders: Al_2O_3 and Al_2O_3-doped Y-PSZ.

Y-PSZ particles was different with respect to that of Al_2O_3: Al_2O_3 particles showed smooth and sharp edges while Al_2O_3-doped Y-PSZ presented round and rough ones; this last shape contributed to an increase in the S_g of Al_2O_3-doped Y-PSZ

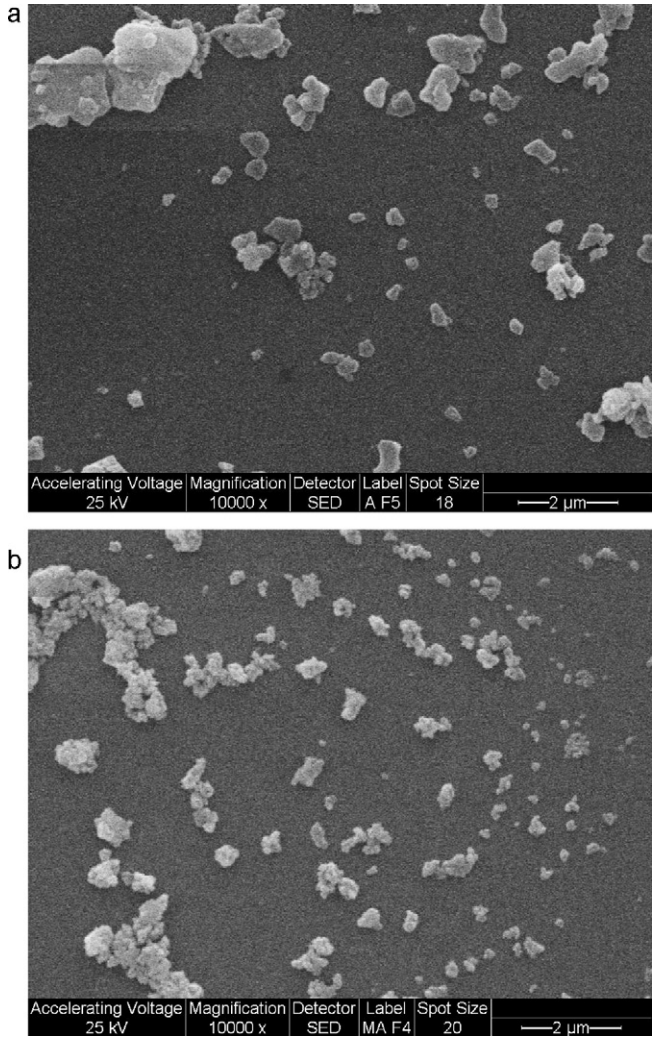

Fig. 2. SEM micrographs of different powders: (a) Al_2O_3 and (b) Al_2O_3-doped Y-PSZ.

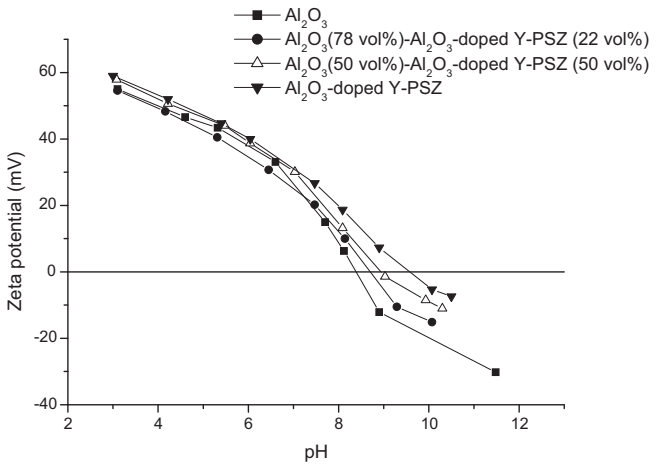

Fig. 3. Zeta potential versus pH curves of Al_2O_3, Al_2O_3-doped Y-PSZ, Al_2O_3 (78 vol%)–Al_2O_3-doped Y-PSZ (22 vol%) and Al_2O_3 (50 vol%)–Al_2O_3-doped Y-PSZ (50 vol%).

powder. As we have mentioned Y-PSZ powder contained 0.3 wt% Al_2O_3, phase equilibrium studies have shown that Al_2O_3 and ZrO_2 are compatible [9]; Al_2O_3 does not form solid solution with zirconia due to its low solubility, therefore a surface coating of Al_2O_3 on ZrO_2 is expected. As the particle size distribution curves of Al_2O_3 and Al_2O_3-doped Y-PSZ were similar (Fig. 1), the higher specific surface area of Al_2O_3-doped Y-PSZ powder with respect to that of Al_2O_3 could be attributed to the particle shape and the Al_2O_3 surface coating.

Fig. 3 shows the zeta potential versus pH curves of Al_2O_3, Al_2O_3-doped Y-PSZ and the two mixtures. The IEP of Al_2O_3 and Al_2O_3-doped Y-PSZ powders was found to be 8.5 and 9.4, respectively. The Al_2O_3 IEP was in agreement with that reported in the literature for this powder [10]; however, the IEP of the Al_2O_3-doped Y-PSZ powder was higher than that reported for commercially available Y-PSZ powders, which showed an IEP value of about 4–6 [2]. The pH_{IEP} values of Al_2O_3 (78 vol%)–Al_2O_3-doped Y-PSZ (22 vol%) and Al_2O_3 (50 vol%)–Al_2O_3-doped Y-PSZ (50 vol%) were 8.7 and 9, respectively; which corresponded to intermediate values between the pH_{IEP} of Al_2O_3 and Al_2O_3-doped Y-PSZ. Thus, a slightly displacement of the Al_2O_3 IEP to higher values was found by substituting Al_2O_3 for Al_2O_3-doped Y-PSZ in the mixtures; as a consequence the negative surface charge of the mixtures at pH 9 decreased. As the Al_2O_3-doped Y-PSZ content increased from 0 to 50 vol%, the magnitude of the negative zeta potential at pH 9 decreased from −13 to −0.77 mV, respectively.

Fig. 4 shows the mean particle diameter (d_{50}) as a function of pH for Al_2O_3 and Al_2O_3-doped Y-PSZ powders. Al_2O_3 could be dispersed at pH values<6.5; the d_{50} increased with increasing pH from 6.5 to 7.5, then it remained nearly constant with further increasing in pH. In the pH range from 3 to 6 the particles became well dispersed indicating an increase in the electrostatic repulsion between particles. At pH > 6 a reduction in the electrostatic repulsion between particles was expected due to the strong flocculation; the Van der Waals attraction forces were dominant and caused aggregation of the particles. This

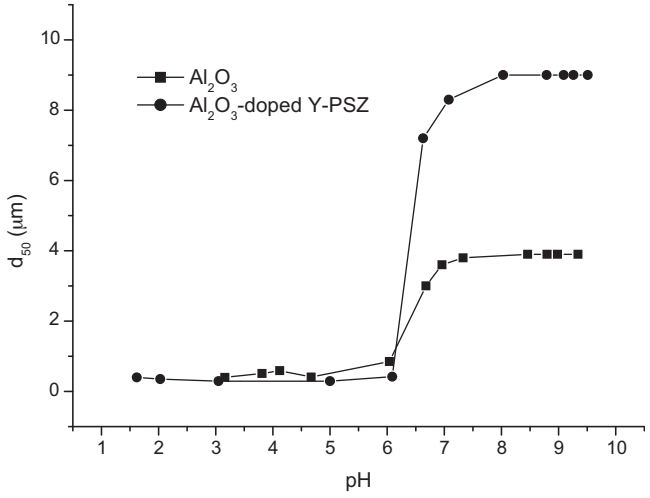

Fig. 4. Mean particle diameter (d_{50}) as a function of pH for Al_2O_3 and Al_2O_3-doped Y-PSZ powders.

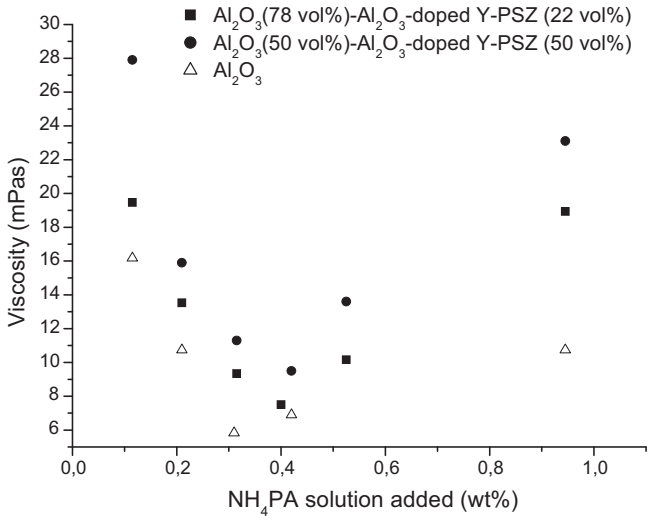

Fig. 5. Viscosity of 35 vol% slips at a shear rate of 542 s^{-1} as a function of the amount of NH_4PA solution added at pH 9 for the different compositions.

aggregation still remained up to pH 9.6 indicating a low negative surface charge of the Al_2O_3 powder in the basic pH region.

The aqueous dispersion of Al_2O_3-doped Y-PSZ was similar to that of Al_2O_3: Al_2O_3-doped Y-PSZ powder could be dispersed at pH values < 6.5; aggregation between particles occurred in the pH range 7.5–9.6, within this pH range the size of Al_2O_3-doped Y-PSZ flocs was approximately twice larger than that of Al_2O_3. The d_{50} versus pH curves were consistent with the zeta potential measurements: (1) Al_2O_3 and Al_2O_3-doped Y-PSZ powders could be dispersed at pH < 6.5 due to the high positive zeta potential, (2) the magnitude of the powders zeta potential in the pH region 7.5–9.6 was not high enough to impart stability to the suspensions. The degree of particle aggregation in aqueous dispersion was determined by the magnitude of the powder surface charge and the Hamaker constant. Since the magnitude of the powders surface charge in the flocculated suspensions (pH 7.5–9.6) was low, the stronger attraction between Al_2O_3-doped Y-PSZ particles and consequently the larger size of their flocs with respect to Al_2O_3 could be attributed to the higher value of the Hamaker constant for Y-PSZ, which was about twice higher than that for Al_2O_3 [11].

3.2. Optimum NH_4PA concentration, amount of NH_4PA adsorbed and zeta potential for the different compositions

Fig. 5 shows the viscosity of 35 vol% slips at a shear rate of 542 s^{-1} as a function of the amount of NH_4PA solution added at pH 9 for the different compositions: Al_2O_3, Al_2O_3 (78 vol%)–Al_2O_3-doped Y-PSZ (22 vol%) and Al_2O_3 (50 vol%)–Al_2O_3-doped Y-PSZ (50 vol%). The optimum NH_4PA concentration, i.e. that which gave slips with the lowest viscosity, was 0.31, 0.4 and 0.42 wt% (dry weight basis of powder) for Al_2O_3, Al_2O_3 (78 vol%)–Al_2O_3-doped Y-PSZ (22 vol%) and Al_2O_3 (50 vol%)–Al_2O_3-doped Y-PSZ (50 vol%), respectively. Differences in the viscosity values were observed for all the compositions throughout the whole range of amount of NH_4PA solution added.

Fig. 6 shows the amount of NH_4PA adsorbed for 35 vol% slips with the optimum NH_4PA concentration as a function of Al_2O_3-doped Y-PSZ content in the mixtures. The adsorption of the polyelectrolyte increased from 0.20 to 0.60 mg/m^2 with increasing Al_2O_3-doped Y-PSZ concentration from 0 to 50 vol%, respectively. As was previously shown (Section 3.1) the increase in the Al_2O_3-doped Y-PSZ content in the mixtures from 0 to 50 vol%, decreased the magnitude of the negative zeta potential at pH 9 from −13 to −0.77 mV, respectively. Consequently, the electrostatic repulsion between the negatively charged powders and the anionic polymer decreased with increasing Al_2O_3-doped Y-PSZ content, thereby increasing the amount of NH_4PA adsorbed. This behaviour is not of "high-affinity type" [12]; the electrostatic repulsion at the surface imparts a barrier for adsorption which limits adsorption to low amounts [8]. However, the fact that adsorption occurred under these conditions indicated that there was a "specific" or "chemical" segment–surface interaction which overcompensated the repulsive electrostatic

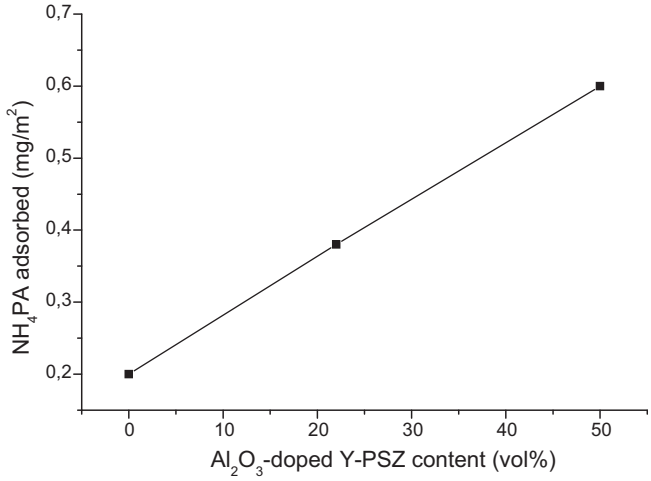

Fig. 6. Amount of NH_4PA adsorbed for 35 vol% slips with the optimum NH_4PA concentration as a function of Al_2O_3-doped Y-PSZ content.

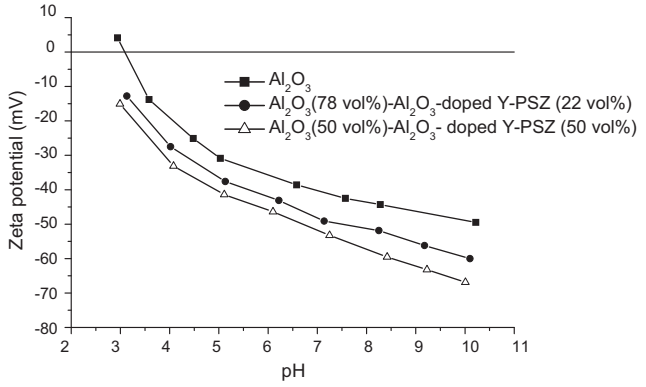

Fig. 7. Zeta potential versus pH curves of different slips with the optimum amount of NH_4PA solution added.

forces. Previous studies on alumina [13] and coated silicon nitride [14], also found a detectable adsorption of anionic polyelectrolytes when the polyelectrolyte and the surface had the same charge sign.

Fig. 7 shows the zeta potential versus pH curves of different slips with the optimum amount of NH_4PA solution added. The adsorption of NH_4PA shifted the Al_2O_3 and mixtures curves without NH_4PA (Fig. 3) towards lower pH values, the IEP for Al_2O_3 was shifted from pH 8.5 to 3.14 and that for Al_2O_3 (78 vol%)–Al_2O_3-doped Y-PSZ (22 vol%) and Al_2O_3 (50 vol%)–Al_2O_3-doped Y-PSZ (50 vol%) to pH values lower than 3. The increase in the magnitude of the negative zeta potential in the pH range 3.25–10.1 with increasing Al_2O_3-doped Y-PSZ content was attributed to the greater amount of NH_4PA adsorbed. As the Al_2O_3-doped Y-PSZ concentration in the mixtures increased from 0 to 50 vol%, the zeta potential at pH 9 increased from −45 to −63.2 mV, respectively. The adsorption of the negatively charged polyelectrolyte enhanced the negative surface charge of the powders. In addition, at pH 9 the electrostatic repulsion between the charged carboxylate groups prevents the accumulation of groups at the surface, the polyelectrolyte adsorbs in a stretched-out configuration which results in long-range steric interactions of the NH_4PA at the solid–liquid interface [12]. Thus, the adsorbed molecules increased the electrosteric repulsion between particles, consequently the slip viscosity attained the minimum value (Fig. 5). At the optimum NH_4PA concentration the suspension was dominated by repulsive forces, thus, it was stabilized.

3.3. Rheological properties

Fig. 8a shows the viscosity at 542 s^{-1}versus the solid loading for different slips: Al_2O_3 with 0.31 wt% NH_4PA, Al_2O_3 (78 vol%)–Al_2O_3-doped Y-PSZ (22 vol%) with 0.4 wt% NH_4PA and Al_2O_3 (50 vol%)–Al_2O_3-doped Y-PSZ (50 vol%) with 0.42 wt% NH_4PA at pH 9. The measured flow curves were satisfactorily fitted with the Casson model ($R = 0.99$). The Casson model equation is:

$$\tau^{1/2} = \tau_0^{1/2} + (\eta_p \gamma)^{1/2} \quad (1)$$

where τ is the shear stress, γ is the shear rate, τ_0 is the yield stress and η_p represents the limiting viscosity at a high shear rate range. The particles in a flocculated suspension form floc groups or a network, because of the mutual attraction between particles; the aggregated particles make the suspension difficult to flow, thereby increasing the τ_0 value [8]. Consequently, the τ_0 value of the Casson model could be used as a parameter that indicated the degree of aggregation and consequently the degree of slip flocculation. The effect of the solid loading on the τ_0 value is shown in Fig. 8b.

The slip viscosity and τ_0 increased with increasing the solid content; an important increase in the viscosity and yield stress were observed for suspensions with a volume percentage of solids higher than about 40 vol%. As the solid content increases particles are forced to approach each other and overlap their

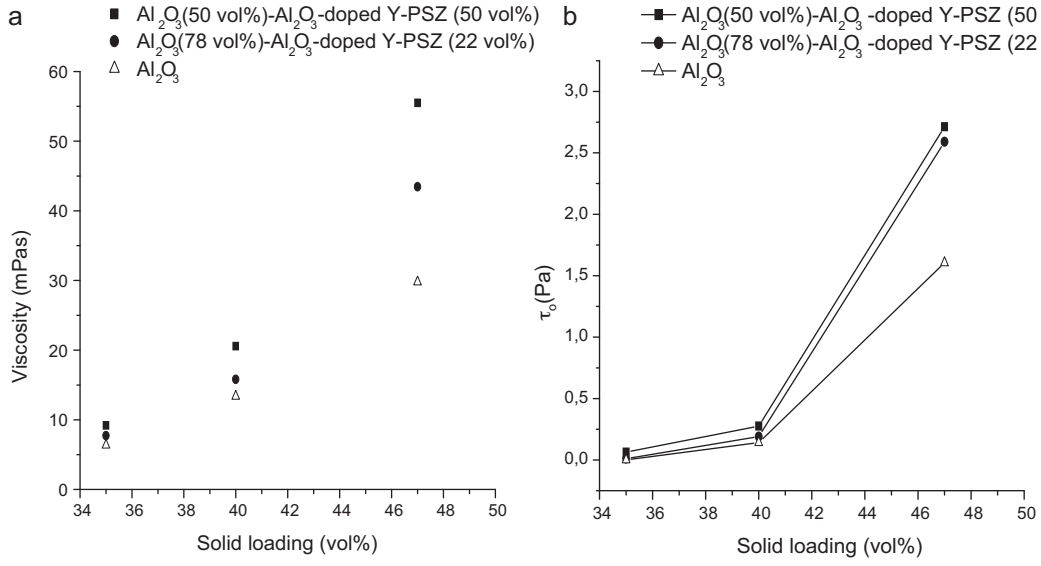

Fig. 8. Viscosity at 542 s^{-1} (a) and τ_0 (b) versus the solid loading for different slips: Al_2O_3 with 0.31 wt% NH_4PA, Al_2O_3 (78 vol%)–Al_2O_3-doped Y-PSZ (22 vol%) with 0.4 wt% NH_4PA and Al_2O_3 (50 vol%)–Al_2O_3-doped Y-PSZ (50 vol%) with 0.42 wt% NH_4PA at pH 9.

electrical double layers (electroviscous effect), thereby decreasing the electrostatic potential and consequently increasing the slip viscosity [15]. Besides, as the repulsion between particles decreases the number of flocs increases, as well as the quantity of entrapped liquid not available for flow [15]. The increase in the yield stress with increasing solid loading was attributed to a higher frequency of the collisions between separate particles, increasing the number of flocs and consequently the resistance to flow. At concentrations > 47 vol% the mean distance between particles decreased, consequently, the adsorbed polymeric layers were in close contact with each other and, the particle interlocking prevented the suspension from flowing. Zupancic et al. [16] observed a similar influence of the particle concentration on the rheological properties of aqueous α-alumina suspensions.

For all the solid concentrations studied, the viscosity and τ_0 values increased with increasing Al_2O_3-doped Y-PSZ content in the mixtures; this behaviour tended to be more pronounced with increasing solid loading. As the Al_2O_3-doped Y-PSZ concentration increased from 0 to 50 vol%, the viscosity of 47 vol% slips increased from 30 to 57.5 mPa s, respectively.

A higher negative zeta potential with increasing Al_2O_3-doped Y-PSZ content from 0 to 50 vol% was observed (Fig. 7); however, a lower viscosity of the mixtures that were more Al_2O_3-doped Y-PSZ rich was not found. This behaviour could be explained taking into account the particle interaction size concept. The calculated volume fraction of solids corresponded to the solid loading of the slurries and did not consider the thickness of hydrated and adsorbed layers around the particles. The distinction between hard size and interaction size becomes important when high solid loading and/or particles with high specific surface area are used [15]. Since the specific surface area of the Al_2O_3-doped Y-PSZ particles was markedly higher than that of Al_2O_3, a greater thickness of hydrated layers surrounding the Al_2O_3-doped Y-PSZ particles was expected. Besides, the substitution of Al_2O_3 by Al_2O_3-doped Y-PSZ increased the thickness of polymer adsorbed (Fig. 6). As a result, the interaction size of the Al_2O_3-doped Y-PSZ particles could be assumed to be larger than that of Al_2O_3. Therefore, as the Al_2O_3-doped Y-PSZ content in the mixtures increased the effective volume fraction at a given solid loading also increased and the amount of free-liquid available for flow decreased, thereby increasing the slip viscosity.

3.4. Sedimentation measurements

Fig. 9 shows the maximum packing fraction (Φ_m) as a function of the solid loading for the different compositions. For all the compositions, Φ_m increased with increasing solid content. The curves were opposite to those of the viscosity versus solid loading (Fig. 8a), slips with low viscosities gave a more dense packing under gravity. In the stable suspensions, the particles could pack in an ordered way, due to the repulsive forces existing between them; the low deposition rate also enabled each particle to search for energetically favourable positions. In this condition, dense packing of particles could be obtained. As the slip viscosity increased, the deposition rate of the particles increased; hence, the searching of one particle for a low energy position was disturbed by the new incoming particles, and the time allowed for particle rearrangement was insufficient. Consequently, a less dense particle packing could be expected. Φ_m values for 47 vol% suspensions prepared from Al_2O_3, Al_2O_3 (78 vol%)–Al_2O_3-doped Y-PSZ (22 vol%) and Al_2O_3 (50 vol%)–Al_2O_3-doped Y-PSZ (50 vol%) were 61, 59 and 55.5%, respectively.

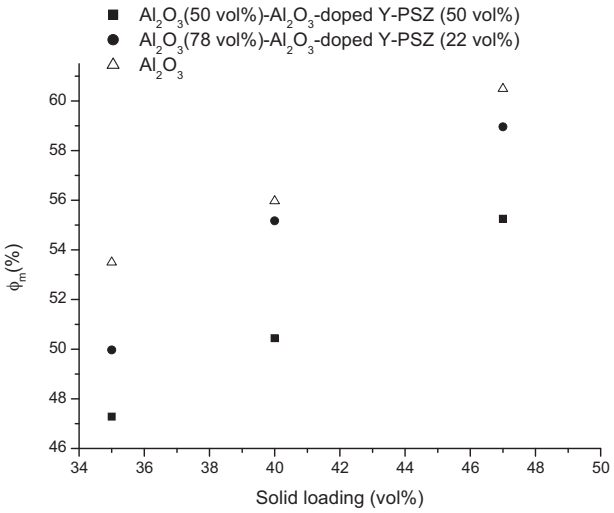

Fig. 9. Maximum packing fraction (Φ_m) as a function of the solid loading for the different compositions.

4. Conclusions

The influence of 0.3 wt% Al_2O_3-doped Y-PSZ concentration on the rheological properties of aqueous Al_2O_3–Al_2O_3-doped Y-PSZ suspensions was studied. Al_2O_3 and Al_2O_3-doped Y-PSZ powders had a similar particle size distribution; however, the particle shape and the surface coating of alumina conferred a markedly higher specific surface area to the Al_2O_3-doped Y-PSZ powder. The substitution of Al_2O_3 by Al_2O_3-doped Y-PSZ in the mixtures decreased the negative surface charge of the powders at pH 9, thereby increasing the amount of NH_4PA adsorbed and consequently the electrosteric repulsion between particles. However, the viscosity and yield stress values increased with increasing Al_2O_3-doped Y-PSZ content for all the solid loading studied. This could be explained by a larger interaction size of the Al_2O_3-doped Y-PSZ particles which resulted in a higher effective volume solid fraction and a lower amount of free-liquid available for flow.

References

[1] J. Wang, R. Stevens, Review zirconia-toughened alumina (ZTA) ceramics, J. Mater. Sci. 24 (10) (1989) 3421–3440.
[2] S. Olhero, I. Ganesg, P. Torres, F. Alves, J.M.F. Ferreira, Aqueous colloidal processing of ZTA composites, J. Am. Ceram. Soc. 92 (1) (2009) 9–16.
[3] C. Piconi, G. Maccauro, Zirconia as a biomaterial, Biomaterials 20 (1999) 1–25.

[4] Y. Shin, Y. Rhee, S. Kang, Experimental evaluation of toughening mechanism in alumina–zirconia composites, J. Am. Ceram. Soc. 82 (5) (1999) 1229–1232.
[5] H.J. Hannink, P.M. Kelly, B.C. Muddle, Transformation toughening in zirconia-containing ceramics, J. Am. Ceram. Soc. 83 (3) (2000) 461–487.
[6] A.H. De Aza, J. Chevalier, G. Fantozzi, M. Schehl, R. Torrecillas, Crack growth resistance of alumina, zirconia and zirconia toughened alumina ceramics for joint prostheses, Biomaterials 23 (2002) 937–945.
[7] J. Cesarano III, I.A Aksay, A. Bleier, Stability of aqueous α-alumina suspensions with poly(methacrylic acid) polyelectrolyte, J. Am. Ceram. Soc. 71 (4) (1988) 250–255.
[8] H. Guldberg-Pedersen, L. Bergstrom, Stabilizing ceramic suspensions using anionic polyelectrolytes: adsorption kinetics and interparticle forces, Acta Mater. 48 (1988) 4563–4570.
[9] F.F. Lange, D.J. Green, Effect of inclusion size on the retention of tetragonal ZrO_2: theory and experiments, Adv. Ceram. Sci. Technol. Zirconia 3 (1981) 222–223.
[10] M.P. Albano, L.B. Garrido, Improvement in the colloidal processing of concentrated silicon nitride slips with ammonium polyacrylate by an yttria–alumina surface coating, Colloids Surf. A 248 (2004) 1–8.
[11] L. Bergström, Adv. Colloid Interface Sci. 70 (1997) 125–169.
[12] D. Liu, S.G. Malgham, Role of polyacrylate in modifying interfacial properties and stability of silicon nitride particles in aqueous suspensions, Colloids Surf. A 110 (1996) 37–45.
[13] J. Cesarano III, I.A. Aksay, Processing of highly concentrated aqueous α-alumina suspensions stabilized with polyelectrolytes, J. Am. Ceram. Soc. 71 (12) (1988) 1062–1067.
[14] M.P. Albano, L.B. Garrido, A.B. Garcia, Dispersion of aluminium hydroxide coated Si_3N_4 powders with ammonium polyacrylate dispersant, Colloids Surf. A 181 (2001) 69–78.
[15] G. Tari, M.F. Ferreira, Lyckfeldt, Influence of the stabilising mechanism and solid loading on slip casting of alumina, J. Eur. Ceram. Soc. 18 (1998) 479–486.
[16] A. Zupancic, R. Lapasin, A. Kristoffersson, J. Eur. Ceram. Soc. 18 (1998) 467–477.